3 RESEARCH PAPER

Apparatus for Testing Concrete under Multiaxial Compression at Elevated Temperature (mac²ᵀ)

4
5

6 **M. Petkovski · R.S. Crouch · P. Waldron**

11 **Abstract** This paper describes a new test facility for
12 determining material mechanical properties of struc-
13 tural concrete. The novel facility subjects 100 mm
14 cubic concrete specimens to true multiaxial compres-
15 sion ($\sigma_1 \neq \sigma_2 \neq \sigma_3$) up to 400 MPa at temperatures of
16 up to 300°C. Forces are delivered through three
17 independent loading frames equipped with servo-
18 controlled hydraulic actuators creating uniform dis-
19 placement boundary conditions via rigid platens.
20 Specimen deformation is calculated from displace-
21 ments measured to an accuracy of 10^{-6} m using a
22 system of six laser interferometers. The combination of
23 stiff loading frames, rigid platens, an accurate and
24 reliable strain measurement system and a fast control
25 system enables investigation of the material response
26 in the post-peak range. The in-house developed con-
27 trol software allows complex multi-stage experiments
28 involving (i) load and temperature cycling, (ii) small
29 stress probes and (iii) arbitrary (pre-defined) loading
30 paths. The program also enables experiments in which
31 the values of the control parameters and the execution
32 of the test sequences depend on the response of the
33 specimen during the test. The capabilities of the
34 facility are illustrated in this paper by experiments
35 determining the effects of different heat-load regimes
36 on the strength and stiffness of the material and tests
37 identifying the tangent stiffness matrix of the material
38 and the associated changes in the acoustic tensor under
39 multiaxial compression.

40 **Keywords** Test facility · Multiaxial compression ·
41 Concrete · Elevated temperature

M. Petkovski (✉) · R.S. Crouch · P. Waldron
Q1 The University of Sheffield
e-mail: m.petkovski@sheffield.ac.uk

Introduction

42

The lack of a comprehensive database of stress and
43
strain measurements on structural concrete under true
44
multiaxial compression is one of the main obstacles
45
preventing the development of reliable constitutive
46
models for this important engineering material. Cur-
47
rent design methods typically assume that the concrete
48
in a column, beam or slab-like structural member is
49
under essentially a uniaxial state of stress. The one-
50
dimensional stress-strain relationship under such con-
51
ditions is often idealised as following a parabolic form,
52
broadly fitting data from uniaxial compression tests.
53
However, in many safety-critical structures (such as
54
nuclear reactor vessels, nuclear containment vessels,
55
offshore platforms and arch-gravity dams) the stress
56
state is most certainly not uniaxial throughout. Engi-
57
neering precision and understanding is lost when the
58
effects of confinement and the deformation behaviour
59
in the other two principal directions are ignored.
60
Furthermore, a constitutive model embracing the full
61
three-dimensional behaviour is a requirement when
62
attempting accurate continuum FE simulations.
63

Although the differences between the uniaxial and
64
biaxial compressive strengths are not so marked, the
65
fracture modes can be quite different [1-3]. Yet it is
66
when all three principal stresses are compressive that
67
very significant differences in strength, deformation and
68
apparent ductility are seen. Most of the knowledge on
69
the behaviour of concrete under multiaxial compression
70
has been gathered from axisymmetric triaxial tests on
71
cylindrical specimens. Triaxial rigs using the Hoek cell
72
[4], originally developed for testing rock, provide
73
simple and inexpensive devices that have proved pop-
74
ular for researchers investigating the response of con-
75
crete under confinement [5–7]. Newman's triaxial
76

compression and extension tests [8], carried out in a specially designed apparatus operating at higher pressures, revealed the dramatic effect of confinement on the stress-strain nonlinearity of concrete. The strains he measured at peak stress were over 57 times larger than those seen under uniaxial compression. The triaxial cell tests performed by Jamet et al. [9] showed that with the increase of confinement the post-peak behaviour of micro-concrete gradually changed from brittle to ductile. Similar change in behaviour was observed in tests on concretes with three different strengths carried out in the Colorado triaxial cell [10]. These tests indicated that for higher strength concretes the transition from brittle to ductile behaviour occurred at higher levels of confinement. In 1999 Lee and Ansari [11] calibrated their constitutive model using data from tests on high-strength concrete in a cell allowing up to 83 MPa confinement and 574 MPa axial stress. In 2002 Sfer et al. [12] tested larger (150 mm diameter, 300 mm long) cylinders in a triaxial cell with a capacity of 4.5 MN axial load and 140 MPa confinement pressure. These tests confirmed the transition from brittle to ductile behaviour and suggested that with the increase of confinement the rupture mode changed from a diffuse distribution of microcracks to a mechanism involving fewer macrocracks separating the specimen into two or three blocks. This was in contrast to the earlier findings of Newman, which suggests that a particular care is needed in interpreting the effects of the boundary conditions at the specimen-platen interface. Other triaxial cells introducing improvements of the original Hoek Cell design include the facilities in Milan and Bergamo [13] and the recently developed GIGA triaxial cell in Grenoble, a rig capable of delivering up to 2500 MPa axial stress on 70 mm diameter, 140 mm long cylindrical specimen, at confinements of up to 850 MPa [14].

While providing important information on the effect of confinement, the triaxial cells are constrained to operate on the compression and extension meridians (that is, the Lode angle is either $+\pi/6$ or $-\pi/6$). The first efforts in true multiaxial compression testing of concrete were made over thirty-five years ago by researchers at the University of New Mexico [15]. They developed an apparatus comprising three independent frames with rigid platens, using polyethylene pads and grease to reduce the platen constraint. Manually operated, pressure controlled actuators with a load capacity of 270 kN were used to test 57 mm cubic specimens under stresses of up to 105 MPa. These findings were valuable, although comparisons with conventional triaxial results suggested that the New Mexico rig did not adequately remove platen friction. In the most comprehensive study of concrete under true

multiaxial compression, Scavuzzo [16] performed 67 tests in a fluid platen rig at the University of Colorado. In addition to simple triaxial compression, triaxial extension and multiaxial compression with three different principal stresses, the cubic specimens were tested under cyclic, staircase, piecewise-uniaxial and circular loading paths. However, the Colorado stress-controlled rig was unable to capture any possible strain softening in the material. The stress range of this impressive apparatus was further limited by the use of leather pads inserted between the fluid cushions and the concrete specimens, which led to stress concentration and development of diagonal cracks near the corners of the specimens at relatively low stress levels. It was at the University of Eindhoven that the post-peak response of conventional structural concrete was captured using brush platens within a rig employing three suspended independent loading frames [17]. Although only a few experiments close to the biaxial regime were reported, that careful work clarified the role of local fragmentation and macroscopic dilation on the loss of load-carrying capacity. The results obtained from using different boundary conditions in the Eindhoven rig suggested that PTFE-coated platens provided the lowest friction restraint in the post-peak region [18].

If there exists limited multiaxial data under ambient conditions, then the position is far worse under elevated temperature. The majority of the experiments performed on hot specimens have been restricted to uniaxial compression. The exceptions are the biaxial studies performed in Braunschweig [19, 20] and the 8 torsional confined cylinder tests at Northwestern University [21]. In the latter tests, the aim was to identify the short-term creep response under controlled moisture conditions at temperatures of up to 200°C. Cylindrical specimens with 152 mm diameter were loaded under axial compression (< 10 MPa), lateral confinement (< 10 MPa) and torsionally induced shear (< 4 MPa). Although these experiments were operating in the relatively low-stress range, the apparatus has the capacity to deliver an axial load of 5 MN, a torque of 5.6 kNm and a fluid cell pressure of 138 MPa.

This lack of data on concrete under high levels of multiaxial compression at elevated temperature led to the development of mac^{2T}, the new experimental rig at The University of Sheffield (Fig. 1).

Test Facility for Multi-Axial Compression of Concrete at Elevated Temperature (mac^{2T})

The apparatus for Multi-Axial Compression of Concrete at Elevated Temperature (maccet → mac^{2T}; pro-

Fig. 1. mac^{2T} apparatus for multiaxial compression of concrete at elevated temperature

nounced *masset*) was designed to satisfy four key testing criteria:

(i) Multiaxial compression of 100 mm cubic specimens up to 400 MPa at any Lode angle ($\sigma_1 \neq \sigma_2 \neq \sigma_3$). Delivery of stresses up to 400 MPa was required to allow structural concretes of the type used in existing nuclear power plant reactor and containment vessels (typical uniaxial compressive strength $f_c = 50-60$ MPa) to be loaded to peak under high levels of hydrostatic confinement (over 100 MPa). The specimen size was fixed at 100 mm to ensure that a representative volume was tested when using 20 mm coarse aggregate. These constraints led to a design solution incorporating three independent loading frames each of 4 MN load capacity.

(ii) Ability to test in the post-peak range. Valuable information on the effective ductility and fracture energy can be obtained by monitoring the post-peak response. However, once the maximum stress is attained, there can be a sudden release of energy stored in the loading frames and the specimen. This can lead to an uncontrollable disintegration of the specimen, with loss of load and displacement measurements. In mac^{2T} this effect was minimised by using a combination of compact, stiff loading fra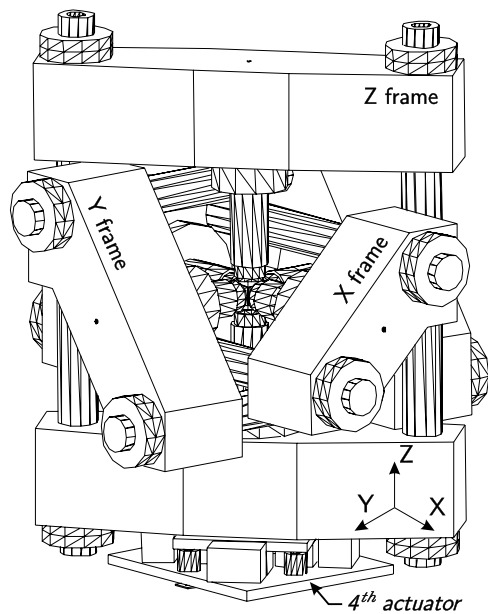mes (reducing the elongation of the tensile bars and bending of the crossheads) and a fast, displacement-controlled servo-hydraulic system that is able to unload the actuators rapidly as the specimen fragments. A disadvantage of rigs where displacements are measured using strain gages bonded to the specimen surface (typical for triaxial cells) is that the large cracks that develop in the post-peak range can fracture the gauges, or local spalling occurs leaving the gauge intact but useless in terms of capturing the global response. This is avoided in mac^{2T} by using un-interruptible laser interferometers that allow an accurate, continuous displacement signal throughout the test.

(iii) Multiaxial compression at temperatures up to 300ºC. The high temperature practically eliminates the fluid platen option and introduces additional requirements on the data acquisition system, such as minimising the effects of temperature variations on strain measurement. In mac^{2T} the loading platens are made of temperature resistant steel (Durehete 1055, 20CrMoVTiB4-10), whereas the thermal effects on the strain measurements are minimised by using a contactless, laser interferometer system.

(iv) Complex multi-stage experiments following arbitrary pre-programmed loading paths with simultaneous temperature cycling. This requirement reflects the desire to generate experimental data for calibrating generalised 3D models able to simulate the response of the material to any combination of loading paths and temperature histories. This was achieved by a custom built system for data acquisition and control with dedicated control software specially developed to meet this requirement.

Other important design requirements were: (v) to minimise the friction on the platen-specimen interface, and (vi) to ensure that the three stresses are delivered centrally on the six faces of the specimen.

Loading and Load Measurement

The load in mac^{2T} is delivered by three 4 MN hydraulic actuators installed in independent, diagonally interlaced loading frames (Fig. 2). This design was chosen to minimise the snap-back potential of the loading frames without increasing the demand on the unloading speed of the servo-hydraulic control system. The high stiffness of the frames was achieved by keeping the tensile bars and the crossheads as short as possible, while allowing sufficient room for the specimen to be installed and removed. Each frame comprises two 200 mm

Fig. 2. mac^{2T} loading frames and 4th actuator

thick steel tiles with 0.25 mm PTFE pads are placed   268
between the loading platens and the concrete speci-   269
men to reduce friction-induced shear stresses at the   270
interface. The loading platens have a spherical seat   271
arrangement to accommodate minor departures in the   272
specimen from a right-regular cube. The 95 mm square   273
loading surface is smaller than the surface of the   274
specimen to prevent contact between adjacent loading   275
platens.   276

One of the actuators (X) has a 180 mm stroke which,   277
when fully retracted, leaves enough space for installing   278
and removing the specimen. The stroke of the other two   279
actuators is 60 mm. The pressure in the system is   280
provided by a 30 MPa hydraulic power unit, which can   281
generate loads up to 3.61 MN (or $\sigma = 400$ MPa over a   282
$95 \times 95\text{mm}^2$ area).   283

A nominally uniform stress field in a (homogenous)   284
specimen can only be achieved by (i) eliminating the   285
friction on the platen-specimen interface, (ii) ensuring   286
that the central axes of the loading platens always   287
cross at the centroid of the specimen and (iii) using   288
precisely machined, right regular cubic specimens. In   289
previous rigid-platen rigs the friction has been reduced   290
by using either greased polyethylene pads (New Mexico   291
[15]) or brush platens (Eindhoven [17]). Polyethylene   292
pads cannot sustain the high temperature levels   293
required in mac^{2T} and, although brush platens have   294
been successfully applied in high-temperature testing   295
(in the biaxial Braunschweig rig [19]), they would not   296
be suitable for post-peak testing where large post-   297
peak deformations may lead to bending and buckling   298

258   diameter steel tensile bars and two 550 mm thick, rolled
259   steel crossheads, one solid, used as a reaction block
260   (supporting the load cell), the other containing the fluid
261   chamber for the hydraulic actuator (Fig. 3). This rep-
262   resents an alternative design solution to that adopted in
263   the six-actuator 250 kN ASTREE apparatus at LMT-
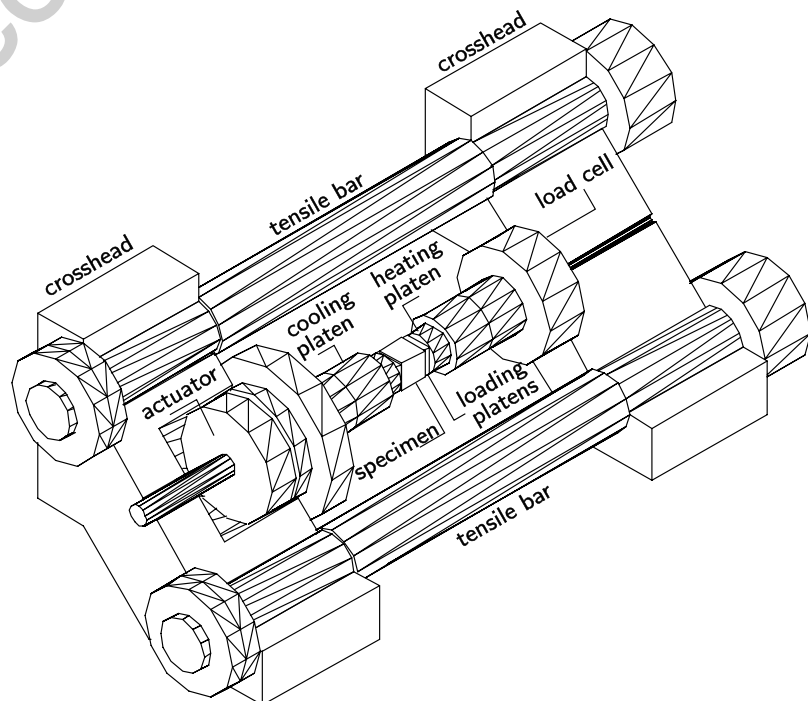264   Cachan [22].
265   The load to the specimen is delivered by 200 mm
266   diameter rams, through a system of cooling, heating
267   and loading platens. In each test, a set of six new 1 mm

Fig. 3. Cross-section of loading frame X

299 of the brushes. PTFE remains stable at temperatures
300 up to 400°C, with very little change in the friction coef-
301 ficient for temperatures between 20°C and 327°C. The
302 0.25 mm PTFE pads, eventually selected for mac²ᵀ,
303 showed no signs of damage at temperatures up to 300°C
304 and stresses of up to 330 MPa.

305   It would be inappropriate to attempt a highly de-
306 tailed FE prediction of the actual stress field operat-
307 ing within a specimen, as the heterogeneity resulting
308 from the stiff aggregate particles (of unknown posi-
309 tion) creates local stress gradients that mask any non-
310 uniform effects from the platen-specimen contact. The
311 decision taken here (common to all such multiaxial ex-
312 perimental work with structural concrete) has been to
313 report nominal stress and strain measures when pre-
314 senting the results.

315   Eccentric loading is prevented by supporting the
316 two horizontal frames (X and Y) on low friction roller
317 bearings, which allow free movement of the crossheads
318 in the horizontal plane. Movement of the centroid of
319 the specimen in the vertical direction (as a result of
320 elastic deformations of the load cell, platens and
321 loading frame) is prevented by active control of the
322 vertical loading frame (Z) position during the tests.
323 This is achieved by an array of 4 linked servo-hydraulic
324 actuators (collectively known as the 4th actuator,
325 installed beneath the Z frame (see Fig. 2) and con-
326 trolled by the difference in the displacements mea-
327 sured at the opposite faces of the specimen. This
328 system contrasts with the ASTREE rig at LMT-
329 Cachan [22], where an actuator and a load cell are
330 used to control/monitor the position/load on each side
331 of the specimen. mac²ᵀ lifts/lowers the entire Z frame
332 to ensure that the specimen centroid remains at the
333 same position within the laboratory throughout the
334 test. Differences in the axial forces from one side of
335 the specimen to the other are minimised through the
336 use of the low friction membranes at the platen-
337 specimen interfaces.

338   The crossheads of the X and Y load frames are
339 supported on 4 reinforced concrete seats bolted to a
340 heavily reinforced concrete slab (Fig. 4). The effects of
341 vibrations induced by machinery operating in the
342 laboratory are reduced by supporting the slab on three
343 columns founded at the lower level (basement) and
344 completely isolated from the floor. Two reinforced
345 concrete columns and an upper crossbeam support
346 vertical guides which keep the Z frame in a vertical
347 plane during re-positioning by the 4th actuator.

348   The applied forces are measured by using three 4
349 MN rated, high precision (± 4 kN) load cells, installed
350 on the reaction side of each frame. These are low-
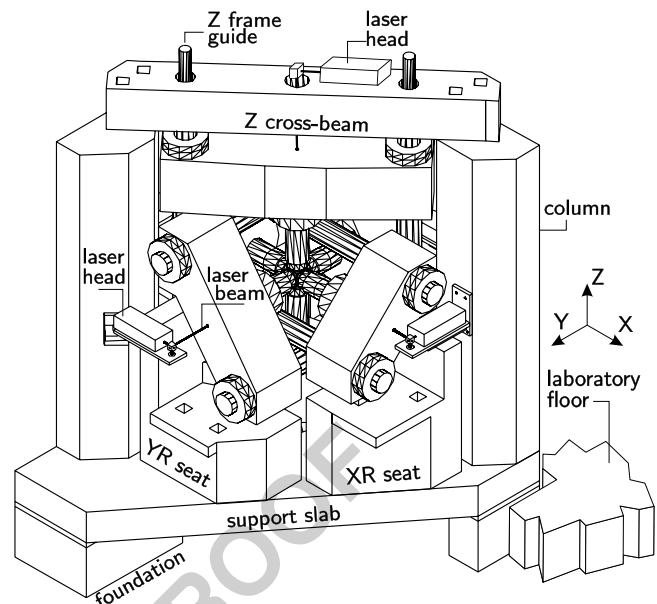351 profile (150 mm), shear-type, 400 mm diameter units,

**Fig. 4.** mac²ᵀ load frames and supports

352 each equipped with two full-bridge strain gauge
353 arrangements. The signal from each bridge is acquired
354 independently and then averaged to provide the
355 process variable for the closed-loop control system
356 (when an axis is under load control). The three load
357 cells are calibrated in the rig, using a separate 3.5 MN
358 load cell, which is itself regularly calibrated at the UK
359 National Physical Laboratory.

360 Displacement and Strain Measurement

361   Positioning of the actuators, all the strain measure-
362 ments and the strain control during the tests are
363 realised by using a system of 6 laser interferometer
364 units. Each unit comprises a laser head (Hewlett
365 Packard, model 5529), a linear interferometer, a linear
366 retro-reflector and a programmable PC calibrator
367 board installed in a dedicated (slave) PC.

368   The retro-reflectors are installed in 18 mm diameter
369 stainless steel tubes, evacuated to 10^{-5} bar, inserted in
370 the 25 mm diameter holes which run through the
371 actuator rams and platens (Fig. 5), as well as through
372 the load cells and crossheads on the reaction side. The
373 vacuum is necessary to reduce turbulent movement of
374 hot air which disturbs the laser beams and may
375 interrupt the measurements. At the specimen end of
376 each of these tubes there is a 5 mm diameter steel pin,
377 which protrudes through the loading platens (including
378 the 1 mm protective steel tile and 0.25 mm PTFE pad)
379 and contacts the face of the specimen directly. Within
380 the tube, the retro-reflector is secured in position at a
381 distance of 47 mm from the tip of the pin. It is just over

Fig. 5 System for strain measurement and displacement control: (**a**) platens with installed vacuum tubes, (**b**) mounting of lasers and (**c**) schematic diagram of laser interferometer system
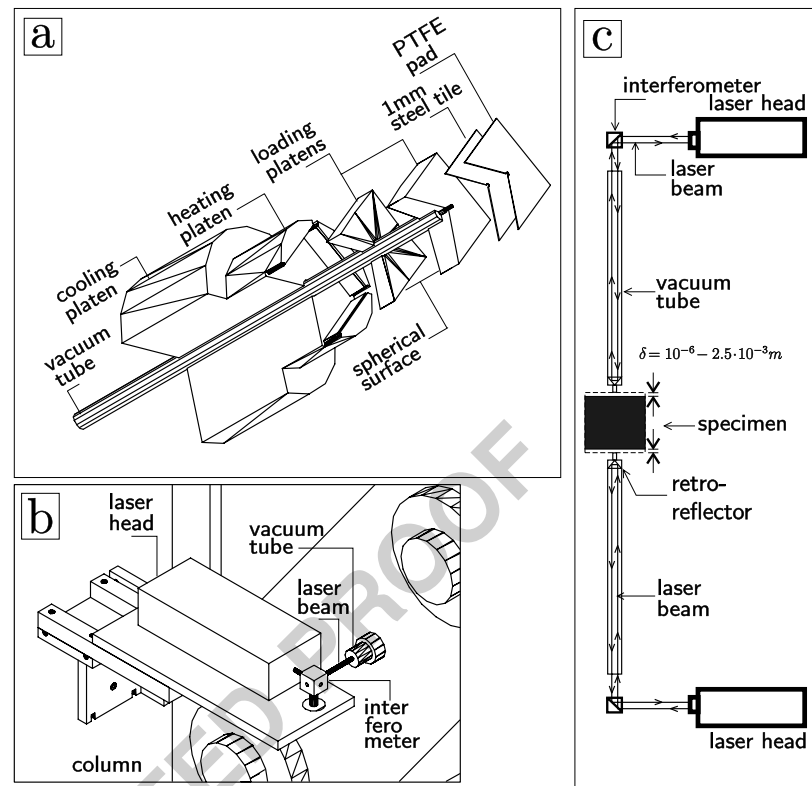
382 this length that thermal expansions and contractions of
383 the pin and the tube have to be calibrated-out during
384 the heating/cooling phases of a test. This setup gives
385 more accurate and reliable results than systems in
386 which the strains are calculated from displacements
387 measured at the ends of long rods [19, 20].

388 This system is capable of measuring large displace-
389 ments with 10^{-6} m accuracy, making it suitable for
390 positioning of the actuators (controlling up to 150 mm
391 of pre-contact movement) and the vertical frame (using
392 the 4th actuator) as well as for strain measurements and
393 strain control during the tests (with displacement rates
394 as low as 10^{-5} m · min^{-1}). In both cases the values ob-
395 tained from the displacement measurement system are
396 used to calculate the process variables for the servo-
397 control system. Strains in the specimen are calculated
398 from the difference between the displacements mea-
399 sured on the opposite faces of the specimen.

400 Heating and Cooling

401 Heat in the rig is generated by a set of six 240 W
402 ceramic band heaters wrapped around the 140 mm
403 diameter steel heating platens [Fig. 5(a)]. Heat is
404 transferred by conduction through the Durehete 1055
405 (20CrMoVTiB4-10) steel loading platens to the speci-

406 mens. The load-cell and actuator are kept cool by
407 flushing cold water through a network of holes cross-
408 drilled through the 200 mm diameter steel cooling
409 platens [Fig. 5(a)].

410 Data Acquisition and Control

411 The system for data acquisition and control of mac^{2T}
412 is integrated into a PC-based solution built around
413 National Instruments hardware and MCC (mac^{2T}
414 Control Centre), a dedicated LabVIEW program for
415 data acquisition and control developed by the first
416 author. The master PC used in the tests is a dual Athlon
417 2 GHz platform equipped with one 24 bit digital input/
418 output board (DIO), two 16 bit multifunction boards
419 (MIO) and one 12 bit analogue output module (AO).

420 All tests in mac^{2T} are monitored by using a total
421 of 49 sensors: (i) 3 load cells (each with 2 indepen-
422 dently monitored full-bridge sensor arrangements),
423 (ii) 6 laser interferometer systems for displacement
424 measurement (both position and specimen deforma-
425 tion), (iii) 1 pressure transducer for monitoring the
426 pressure in the 4th actuator, (iv) 6 linear variable
427 displacement transducers (LVDTs) used as a backup
428 displacement measurement system, (v) 6 LVDTs
429 used to monitor the position of the crossheads and

430 (vi) 24 K-type thermocouples installed on the heating
431 platens (4 per platen).

432 The signals from all analogue devices (LVDTs, load
433 cell bridges, pressure transducer and thermocouples)
434 are first conditioned, then passed to the analogue IO
435 boards where they are converted into digital data at a
436 rate of 500 samples·s^{-1} (multiplexed over 43 channels).
437 In MCC, the acquired data are then averaged in
438 packages of 100 samples at a time. The signals from
439 the laser interferometers are generated as digital data
440 by the six PC calibrator boards installed in the slave
441 PC and transferred to the master PC by the means of
442 digital IO communication controlled from MCC.

443 The averaged input values and the test control param-
444 eters are used for calculating the control variables in the
445 PID (proportional, integral, derivative) modules in
446 MCC. The program outputs are the values of the
447 signals to be sent to the 4 actuator servo-valves and
448 6 temperature controllers. The analogue (voltage)
449 signals are generated by four 16-bit D/A converters of
450 the MIO boards, for the actuators, and six 12-bit D/A
451 converters of the AO module, for the control of the
452 heaters.

Operation of the Rig
453

454 The process of acquiring the data, averaging the
455 values, calculating the control variable and sending
456 the control signal to the servo-valve or temperature
457 controller represents a fully closed control loop. The
458 mac^{2T} rig is operated by 10 independent control loops:
459 3 for the main actuators, 1 for the 4th actuator and 6 for
460 the temperature controllers. The actual time for clos-
461 ing the loops depends on the ratio between the sam-
462 pling rate and the number of averages (0.1 s, for the
463 current hardware and software configuration).

464 In essence, the operation of the rig is controlled by
465 defining three sets of parameters for each of the four
466 actuators: (i) control mode, (ii) process variable (PV),
467 and (iii) rate of change of the PV; and the rate of
468 change of the PV for the temperature controllers.

Control Loops
469

470 The three load frame actuators can be operated in
471 either load (LC) or displacement control (DC) mode.
472 The process variable for load control is the load L
473 calculated as an average of the readings from the two
474 bridges of each load cell. The displacement control can
475 be performed by using one of the three different values
476 as process variables: (i) V-the laser measurements of
477 the actuator position, (ii) dV-the laser measurements

478 of the specimen deformation (difference between the
479 displacements measured at the two opposite faces of
480 the specimen), and (iii) U-the LVDT measurements of
481 the position of the actuators. The diagram of the
482 control loops is shown in Fig. 6.

483 The V-control is used for positioning the actuators
484 before the beginning of the tests (loading) and after the
485 completion of the tests (unloading). The dV-control is
486 used for displacement control during the tests. The
487 U-control is used in a backup (safety) procedure that is
488 automatically triggered in case any of the laser signals is
489 interrupted. Each load frame is controlled indepen-
490 dently, which means that each of the actuators can be
491 under L, V, dV or U-control, regardless of the control
492 mode of the others.

493 The 4th actuator only operates in displacement con-
494 trol, using one of the three process variables. The six
495 heaters are controlled independently with process
496 variables obtained as average values of the temperature
497 measurements obtained from the 4 thermocouples
498 installed on each of the 6 heating platens.

Modes of Operation and Test Stages
499

500 The MCC software is designed to provide two basic
501 modes of operation of the rig: (i) interactive and (ii)
502 automatic. In the interactive mode, the operator con-
503 trols the rig either by manually setting the control pa-
504 rameters (control modes, PV and rates) for each
505 actuator and temperature controller, or by activating a
506 range of different pre-programmed procedures. In the
507 automatic mode, the program reads an input file at the
508 beginning of the test and performs a series of opera-
509 tions, without the need for further intervention from
510 the operator. The automatic procedure can always be
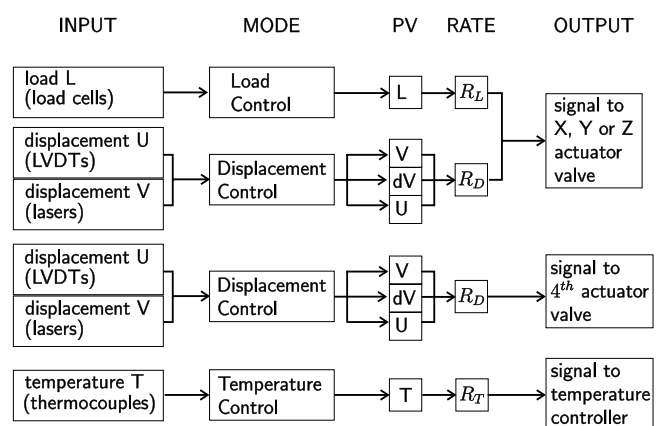511 overridden by the operator and switched into interac-
512 tive mode.

Fig. 6. Operation of mac^{2T}: diagram of control loops

The changes between the control modes are *bumpless* and can be performed at any time during the execution of the test as prescribed by the input file, triggered by the MCC automatically (in case of certain, pre-programmed conditions) or by the operator (in interactive mode). The process variables and rates for each control loop can be also prescribed in the input file, defined by the operator during the test or triggered by the MCC automatically.

Each test is performed in three stages: (i) loading, (ii) testing, and (iii) unloading. Once the specimen is installed in the rig, the operator activates the automatic loading procedure in which the Z frame is lifted into position and the three actuators are extended until the specimen is loaded to contact stress (pre-defined, typically 0.5–1.0 MPa) in all three directions, first Z, then X and finally Y. During this stage, the movement of the Z-frame (4th actuator) and the three loading actuators is controlled by displacements (V-control) with rates decreasing gradually as the platens approach the specimen. Once the contact stress is detected in any of the three directions, the control of that actuator switches to load and the rate of the process variable is set to zero. When all axes are in load control the operator can start the testing stage. Similarly, when the test is finished, the unloading procedure starts by switching the controls to displacement (V) and retracting the actuators in a reverse order: Y, X, Z and finally the 4th actuator, until the Z-frame rests on its base.

In the testing stage the three main actuators are either under load or dV-control, with load/displacement rates prescribed by the pre-programmed test procedure or set by the operator. The 4th actuator is always in dV-control, with variable displacement rates calculated by an MCC module programmed to keep the centroid of the specimen at the same level with the horizontal loading axes during the tests.

Programmed Test Sequences

All mac^{2T} tests can be composed by using six test sequences (procedures) programmed in MCC. Each sequence contains predefined criteria. When these criteria are met, the sequence is completed and the program moves on to the next sequence. The modular structure of the program allows other sequences to be added in the future.

The load cycling in each test is performed by using one of the three different *loading/unloading* procedures: 3LC, 1DC or 2DC.

1. The 3LC procedure, in which the three main actuators are controlled independently in load control, is used for loading/unloading under specified stress conditions at a safe distance from the peak nominal stress (PNS) surface. The sequence is completed when the load in one axis (*leader*) reaches a pre-defined level.

2. 1DC is a procedure in which one axis (σ_1) is under displacement control with a prescribed displacement rate (R_D), whereas the other two axes are in load control, following σ_1 at preset ratios α_2 and α_3. The change of σ_1 is monitored at regular time intervals (t_c), and, assuming that the stress rate remains unchanged during two successive intervals ($\Delta \sigma_1^{i+1} = \Delta \sigma_1^i$), the loading rates for the other two directions ($k = 2, 3$) are calculated as: $R_k = [\alpha_k(\sigma_1^i + \Delta \sigma_1^i) - \sigma_k^i]/(t_c A)$, where A is the loading area. This procedure is used for experiments in which one stress (σ_1) is close to the peak, such as triaxial compression ($\sigma_1 > \sigma_2 = \sigma_3$), or tests in which the three stresses are different ($\sigma_1 > \sigma_2 > \sigma_3$).

3. 2DC is similar to the 1DC procedure, but with two *leader* axes in displacement control (with prescribed rates R_{D1} and R_{D2}) and one in load control. The loading rate in the third axis is calculated in the same way as that in the 1DC procedure, but with the stress rate taken as an average of the stress increments measured in the two *leader* axes.

This procedure is used for close-to-peak testing near the extension meridian, where the stresses in two directions are similar while the stress in the third direction decreases or remains constant ($\sigma_1 \approx \sigma_2 > \sigma 3$).

The two DC procedures are used for testing close to peak and in the post-peak region. They are not suitable for lower stress levels where the specimen is still relatively stiff and even low displacement rates in the *leader* axes can produce high loading rates in the load-controlled axes, possibly resulting in serious over/under shooting of the PID controllers and, ultimately, to loss of control. The execution of the DC sequences is controlled by setting limits to the values of (i) the loading stiffness $S = \Delta \sigma_1 / \Delta \varepsilon_1$ and (ii) ratio between the current stress and the maximum stress recorded during the sequence $\beta = \sigma_1 / \hat{\sigma}_1$; calculated for the *leader* axis (or average of the two *leader* axes in 2DC) at the end of intervals with a predefined duration t_c. The limit of the stress ratio β is always set between 0 and 1. If $S_{lim} > 0$, then the sequence is terminated when $S < S_{lim}$, before the specimen starts softening (pre-peak tests). If $S_{lim} < 0$, then the sequence is terminated when the stress σ_1 drops below $\beta_{lim} \hat{\sigma}_1$ (post-peak tests).

Stress probing procedures are test sequences in which the specimen is loaded/unloaded by a small stress (typically $\Delta\sigma^P = 2 - 3\,\mathrm{MPa}$) in each of the three directions, while the strains in the other two directions are kept constant. The results are used to determine the values of the tangent stiffness and elastic unloading stiffness matrices of the material for a given stress state (at the start of the probing procedure).

4. P3LC is a stress probing procedure in which the three stress probes are performed in load control. When the stress in the probing direction i increases by $\Delta\sigma_i^{\mathrm{Pi}}$, the strain in this direction changes to $\varepsilon_i + \Delta\varepsilon_i^{\mathrm{Pi}}$. The strains in the other two directions are kept constant ($\Delta\varepsilon_j^{\mathrm{Pi}} \approx \Delta\varepsilon_k^{\mathrm{Pi}} \approx 0$) while the stresses change by $\Delta\sigma_j^{\mathrm{Pi}}$ and $\Delta\sigma_k^{\mathrm{Pi}}$, as shown in Fig. 7(a). When the three probes are completed the tangent stiffness matrix **D** is calculated from the stress and strain increments measured during the loading parts of the three probes [see Fig. 7(b)]. The elastic unloading matrix $\mathbf{D_u}$ is calculated in a similar way from the values recorded in the unloading branches of the three probes. After completing the three probes, the stresses are returned to their initial levels recorded at the start of the probing sequence, and the program moves on to the next test sequence.

5. P1DC is a probing sequence in which the loading part of the probe in one direction (σ_1) is performed under displacement control with a given rate R_D. This procedure is used in tests where the major principal stress is greater than the other two stresses and close to the PNS ($\sigma_1 > \sigma_2 \geqslant \sigma_3$). If σ_1 is close to the peak, the loading stiffness of the specimen in the probing direction can be very low (often associated with stress relaxation in the other two directions) and loading to $\sigma_1 + \Delta\sigma_1^{\mathrm{P1}}$ can take a long time. If the specimen is softening, then σ_1 will decrease under displacement control. To avoid very slow loading or softening, the time for the loading part of the probe is limited, resulting in $\Delta\sigma_1^{\mathrm{P1}} < \Delta\sigma^{\mathrm{P}}$ or even $\Delta\sigma_1^{\mathrm{P1}} < 0$ (stress relaxation).

6. P2DC is similar to P1DC, but with two stress probes performed under displacement control. This procedure is used in triaxial extension tests where $\sigma_1 \approx \sigma_2 > \sigma_3$, and the two larger stresses are close to the peak stress levels.

The temperature in the specimen is controlled in all test sequences by specifying the heating rate R_H (in $^\circ\mathrm{C}\cdot\mathrm{min}^{-1}$) and limit temperature T_L. When T_L is reached the program sets R_H to 0.
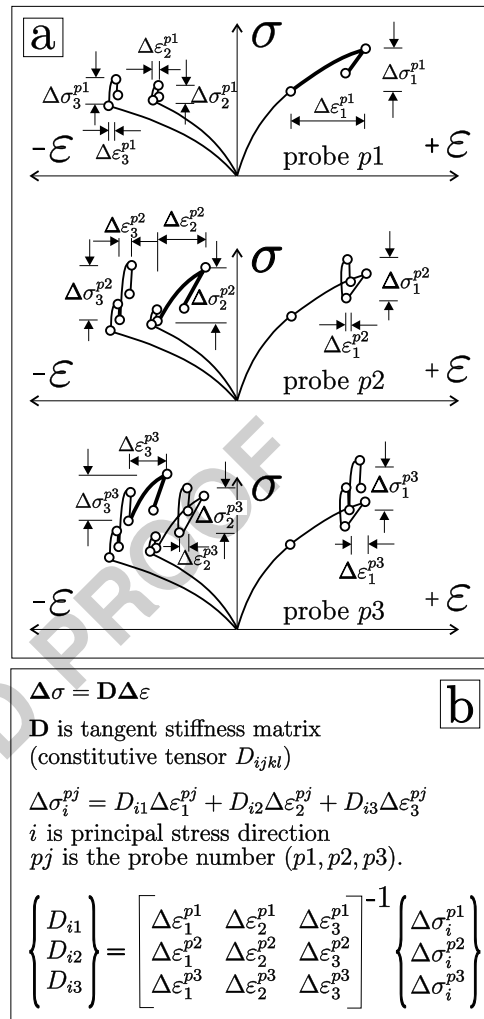

Fig. 7. Stress probing: (**a**) test sequence and (**b**) experimental determination of stiffness matrices

Experimental Testing in mac²ᵀ

A typical elevated temperature test in mac²ᵀ is performed in two phases: (i) *conditioning* and (ii) *deviatoric loading*.

Conditioning Phase

In the *conditioning* phase the specimen is subjected to temperature changes with or without load. When loaded, the specimens are subjected to moderate (service) stresses, typically no higher than 50% of the uniaxial compression strength of the material (f_c). The temperature is either increased monotonically to $\hat{T}$ (up to 300°C) or applied in cycles between ambient and $\hat{T}$, at constant heating/cooling rates between 0.1 and 3°C $\cdot$ min⁻¹. During the heating and cooling stages the temperature inside the specimen lags behind that measured in the platens. Calibration tests on speci-
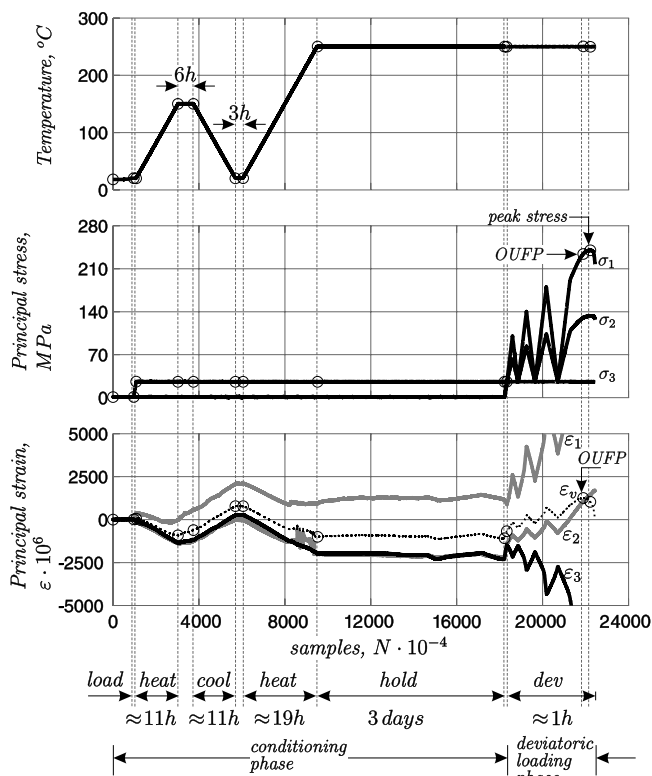
Fig. 8. Typical elevated temperature test in mac^{2T}: histories of temperature, stress and strain

total strains) and to provide a reference for assessing the effects of heat-load regimes on the material behaviour under multiaxial stress.

The time histories of temperature, stress and strain from a typical mac^{2T} L-H test are shown in Fig. 8. The specimen is first loaded in uniaxial compression to 26 MPa, then heated to 150° C, cooled to 20° C, heated to 250° C, and held under steady-state conditions for 3 days before starting the *deviatoric loading* phase.

Deviatoric Loading Phase

The influence of different loading and heating-cooling regimes in the *conditioning* phase on the properties of the material under multiaxial loading are investigated in the second, *deviatoric loading*, phase of the tests.

In the simplest tests, the specimen is loaded in one deviatoric plane (between Lode angles $\pi/6$ and $-\pi/6$), in several cycles with gradually increasing stress
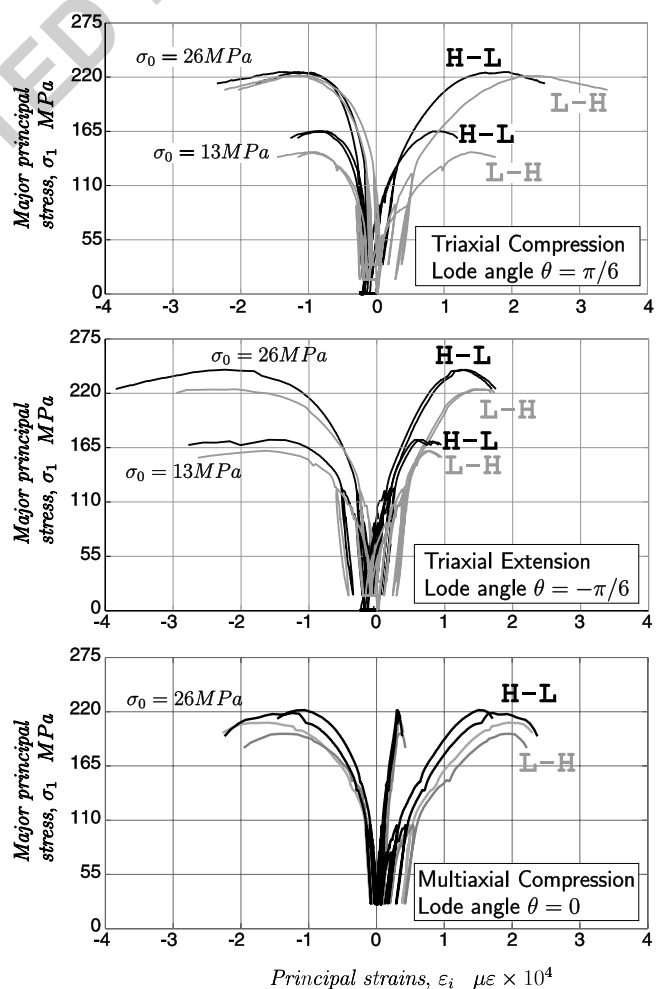
mens with embedded thermocouples showed that the temperatures within the specimen depended on the heating rate and the moisture content of the concrete. For 2 year old concrete kept at room conditions, heated to $\hat{T} = 250°C$ at $2°C \cdot min^{-1}$, the temperatures within the specimen were $190°C$, 10 mm from the surface, and $180°C$, at the centroid, when the platens first reached $250°C$. After maintaining the platen temperature at $250°C$ for 2 hours, the specimen centre reached $236°C$. All *conditioning* phases in the elevated temperature tests performed in mac^{2T} included a period of at least 24 hours holding at constant temperature of $250°C$, at which time the specimen attained a steady state $\approx 248°C$.

Load-then-heat (L-H) tests are used for investigating the load induced thermal strains (LITS), a phenomenon of particular importance for fire engineering and design of concrete structures in nuclear power plants. After each heating and cooling cycle the specimen is held under steady state conditions for short periods until it reaches thermal and hygral equilibrium. In some tests the heating to $\hat{T}$ is followed by longer periods of steady state (up to 5 days), in order to measure creep at constant (elevated) temperature. Heat-then-load (H-L) tests are used to determine drying shrinkage (needed for separating LITS from

Fig. 9. Simple deviatoric loading test in mac^{2T}: stress-strain graphs recorded after heat-load (H-L) and load-heat (L-H) conditioning at two different levels of hydrostatic confinement σ_0

magnitudes, followed by monotonic loading to peak stress (Fig. 9). These tests provide data on the relationship between heating, cooling and loading ($\hat{T}$, heating-cooling rates, heat-load sequence, and stress state during heating-cooling) and multiaxial strength of the material [23], tangent stiffness, elastic unloading stiffness, pre-peak volumetric expansion (or OUFP— onset of unstable fracture propagation), plastic flow and softening behaviour of the material.

More complex deviatoric loading tests include (i) deviatoric load cycles at fixed Lode angles but varying hydrostatic confinement levels and (ii) stress probes at different stress levels in each deviatoric cycle.

In Fig. 10 are shown the loading path and stress-strain response recorded in a triaxial compression test ($\theta = \pi/6$, $\sigma_1 > \sigma_2 = \sigma_3$). The load was applied in six deviatoric planes (normal to the hydrostatic axis ξ), at increasing levels of hydrostatic confinement. The test in each cycle i was carried out in 4 steps: (1) load hydrostatically to a predefined level σ_0^i, (2) load in a deviatoric plane to $\sigma_1 = 0.975\hat{\sigma}^i$, (3) perform probes at
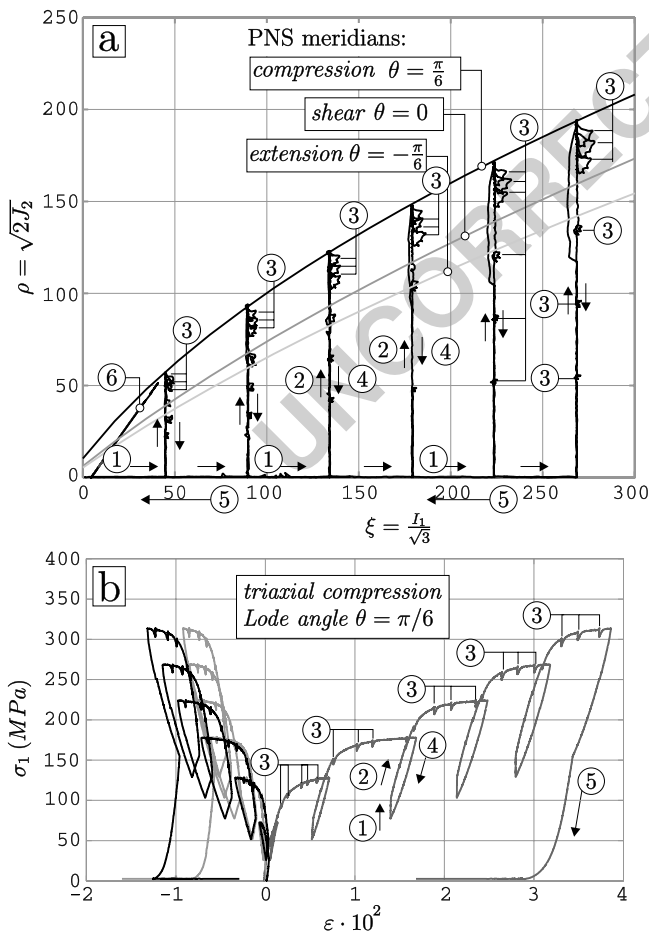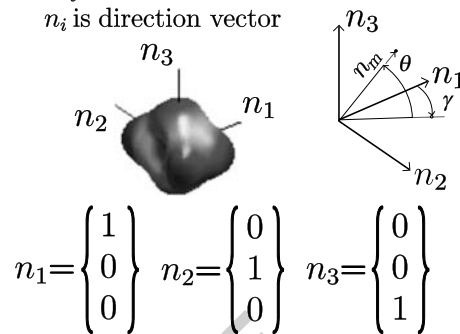
$$Q_{jk} = n_i D_{ijkl} n_l$$

Q_{jk} is acoustic tensor
D_{ijkl} is constitutive tensor
n_i is direction vector

$$n_1 = \begin{Bmatrix} 1 \\ 0 \\ 0 \end{Bmatrix} \quad n_2 = \begin{Bmatrix} 0 \\ 1 \\ 0 \end{Bmatrix} \quad n_3 = \begin{Bmatrix} 0 \\ 0 \\ 1 \end{Bmatrix}$$

Fig. 11. Acoustic tensor surface calculated from experimentally determined stiffness matrices

6 stress levels $\sigma_1 = 0.6, 0.7, 0.8, 0.9, 0.925$ and $0.95\hat{\sigma}^i$, and (4) unload to σ_0^i. After completing the six loading cycles, the specimen was unloaded along the hydrostatic axis (step 5) and tested under σ_3 compression ($\sigma_1 = \sigma_2 = 3$MPa) to determine the residual strength of the material (step 6).

Performing a series of small compression *probes* in each of the three orthogonal directions, while maintaining strains fixed in the other directions, allows the isotropic upper 3×3 sub-matrix of the 6×6 constitutive [D] matrix to be estimated [Fig. 7(b)]. The remaining terms of the [D] matrix were calculated by adopting the original elastic shear modulus. This could have been estimated, for an equivalent isotropic material, from the altered mean Young's modulus and mean Poisson's ratio. However, the effect of not changing the shear modulus was shown to be near-negligible when examining an equivalent elasto-plasticity model. By calculating the acoustic tensor from this matrix, a measure of impending material instability can be determined [24]. This measure (the determinant of the acoustic tensor) has both direction and magnitude, thus it may be represented graphically (Fig. 11) by a surface which starts out as being spherical and evolves (collapses) into a form where the radius becomes zero in the direction normal to the orientation of a newly formed discontinuity surface. Such results give a detailed picture of the material behaviour under multiaxial compression needed for construction of advanced constitutive models.

Fig. 10. Complex deviatoric loading in mac^{2T}: (**a**) loading path and (**b**) stress-strain response of the specimen under multiaxial compression. $I_1 = \mathrm{tr}[\sigma]$ and $2J_2 = \mathrm{tr}[s^2]$

Conclusions

The new mac^{2T} facility was developed to overcome the lack of high quality experimental data on the behav-

iour of concrete under true multiaxial compression, under relatively high levels of confinement, at both ambient and elevated temperature. The fully automated programmable control system allows multi-stage experiments to be carried out by following complex load paths and temperature histories, at any Lode angle and in the post-peak range. These tests provide new macroscopic data needed to construct advanced constitutive models for simulating the response of concrete under generalised stress states. The observed effects of different heating and loading regimes on the evolving mechanical properties provide insight into the stress and temperature-induced changes in the material fabric at a lower, microscopic, level.

References

1. Kupfer HB, Hilsdorf HK, Rusch H (1969) Behaviour of concrete under biaxial stresses. J ACI 66(8):656–666.
2. Liu TC, Nilson AH, Slate FO (1972) Stress-strain response and fracture of concrete in uniaxial and biaxial compression. J ACI 69(5):291–295.
3. Gerstle KH, Aschl H, Bellotti R, Bertacchi P, Kotsovos MD, Ko H-Y, Linse D, Newman JB, Rossi P, Schickert G, Taylor MA, Traina LA, Winkler H, Zimmerman RM (1980) Behaviour of concrete under multiaxial stress states. J Eng Mech, ASCE 106:1383–1403.
4. Franklin JA, Hoek E (1970) Developments in triaxial testing equipment. Rock Mech 2:223–228.
5. Chern JC, Yang HJ, Chen HW (1992) Behaviour of steel fiber reinforced concrete in multiaxial loading. ACI Mater J 89(1):32–40.
6. Attard MM, Setunge S (1996) Stress-strain relationship of confined and unconfined concrete. ACI Mater J 93(5):432–442.
7. Imran I, Pantazopoulou SJ (1996) Experimental study of plain concrete under triaxial stress. ACI Mater J 93(6):589–601.
8. Newman JB (1973) Deformation behaviour, failure mechanisms and design criteria for concrete under combinations of stress, Part IV, PhD Thesis, University of London, 1–583.
9. Jamet P, Millard A, Nahas G (1984) Triaxial behaviour of a micro-concrete complete stress-strain curves for confining pressures ranging from 0 to 100 MPa. In: RILEM-CEB International Conference Concrete under Multiaxial Conditions, INSA Toulouse, 1984, Vol. 1, 133–140.
10. Smith SS, Willam KJ, Gerstle KH, Sture S (1989) Concrete over the top, or: is there life after Peak? ACI Mater J 86(5):491–497.
11. Li Q, Ansari F (1999) Mechanics of damage ond constitutive relationships for high-strength concrete in triaxial compression. J Eng Mech ASCE 125(1):1–10.
12. Sfer D, Carol I, Gettu R, Etse G (2002) Study of the behaviour of concrete under triaxial compression. J Mech Eng ASCE 128(2):156–163.
13. Belloti R, Rosssi P (1991) Cylinder tests: experimental technique and results. Mat Struct 24:45–52.
14. Vu XH, Gabet T, Malecot Y, Daudeville L (2005) Experimental analysis of concrete behaviour under severe triaxial loading. Proc. McMat2005, Joint ASME/ASCE/SES Conference on Mechanics and Materials, Baton Rouge, Louisiana, paper 247, 1–6.
15. Mills LL, Zimmerman RM (1970) Compressive strength of plain concrete under multiaxial loading conditions. ACI Journal, October 1970, 802–807.
16. Scavuzzo R (1982) Behaviour of concrete under multiaxial load histories. MSc Thesis, University of Colorado.
17. Van Mier JGM (1984) Strain softening of concrete under multiaxial loading conditions. PhD Thesis, University of Eindhoven.
18. Van Mier JGM, Vonk RA (1991) Fracture of concrete under multiaxial stress-recent developments. Mat Struct 24:61–65.
19. Ehm C, Schneider U (1985) The high temperature behaviour of concrete under biaxial conditions. Cem Concr Res 15:27–34.
20. Thienel K-Ch, Rostásy FS (1996) Transient creep of concrete under biaxial stress and high temperature. Cem Concr Res 26(9):1409–1422.
21. Bažant ZP, Prasannan S (1986) High-temperature triaxial torsional creep tests of concrete at various hygral conditions. Nucl Eng Des 94:137–151.
22. Calloch S, Marquis D (1999) Triaxial tension-compression tests for multiaxial cyclic plasticity. Int J Plast 15:521–549.
23. Petkovski M, Crouch R, Waldron P (2005) Multiaxial creep and damage under elevated temperature. Concreep 7— International conference on creep, shrinkage and durability of concrete and concrete structures, Nantes, 12–14 September 2005, paper CC7-121, in press.
24. Rudnicki JW, Rice JR (1975) Conditions for localization of deformations in pressure sensitive dilatant materials. J Mech Phys Solids 23:371–394.